Supplemental Information

Operando Investigation of Aqueous Zinc Manganese Oxide Batteries: Multi-Stage Reaction Mechanism Revealed

Daren Wu,[a,b] Steven T. King, [a,c] ,Nahian Sadique,[a,c] Lu Ma,[d] Steven N. Ehrlich,[d] Sanjit Ghose,[d] Jianming Bai,[d] Hui Zhong,[d] Shan Yan,[a,e] David C. Bock,[a,e] Esther S. Takeuchi,[a,b,c,e] Amy C. Marschilok,[a,b,c,e] Lisa M. Housel,[a,e] Lei Wang,[a,e] Kenneth J. Takeuchi,[a,b,c,e]*

*corresponding author: kenneth.takeuchi.1@stonybrook.edu

Affiliations

[a]Institute of Energy: Sustainability, Environment, and Equity, Stony Brook University, Stony Brook, New York 11794, USA
[b]Department of Materials Science and Chemical Engineering, Stony Brook University, Stony Brook, New York 11794, USA.
[c]Department of Chemistry, Stony Brook University, Stony Brook, New York 11794, USA.
[d]National Synchrotron Light Source II, Brookhaven National Laboratory, Upton, New York 11973, USA.
[e]Interdisciplinary Science Department, Brookhaven National Laboratory, Upton, New York 11973, USA.

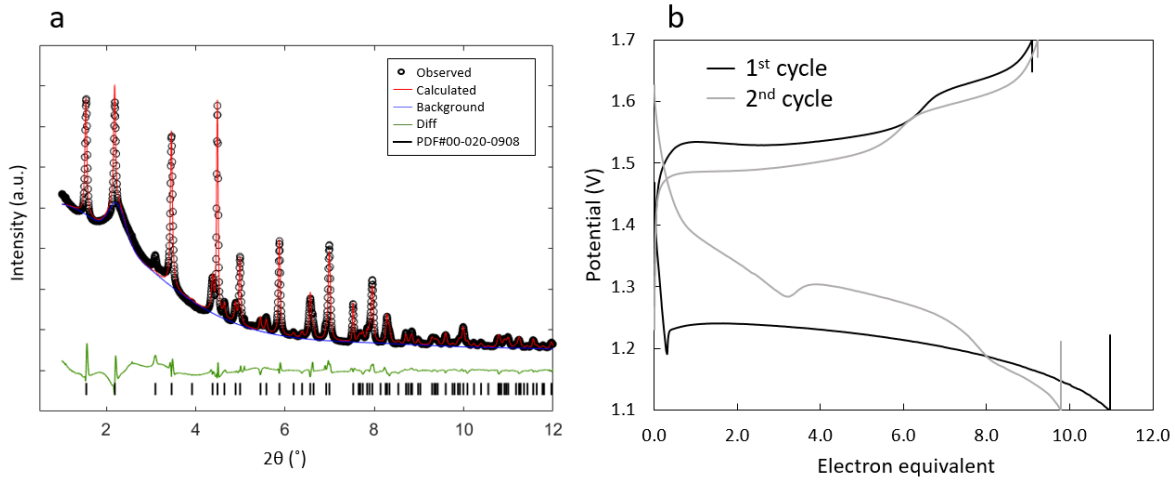

Figure S1 a Synchrotron XRD of the pristine cryptomelane-type α-MnO_2 powder. **b** Cycle 1 and Cycle 2 Galvanostatic potential profiles of Zn/α-MnO_2 cell with 2 M $ZnSO_4$ electrolyte.

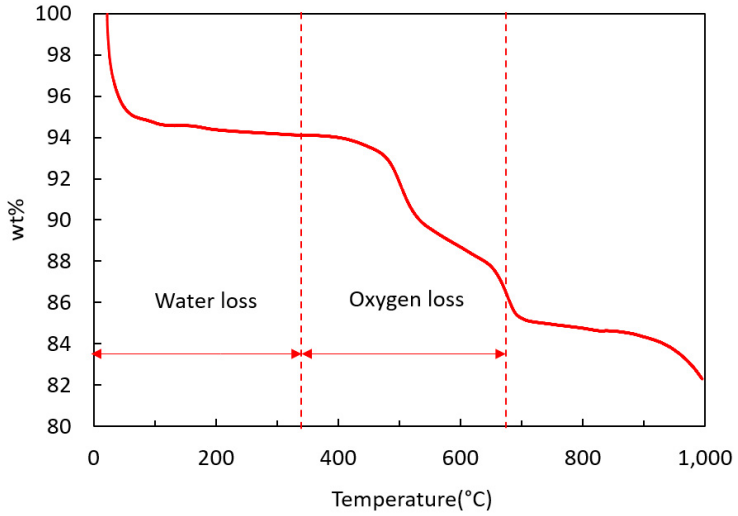

Figure S2 TGA of as-synthesized α-MnO_2 powder.

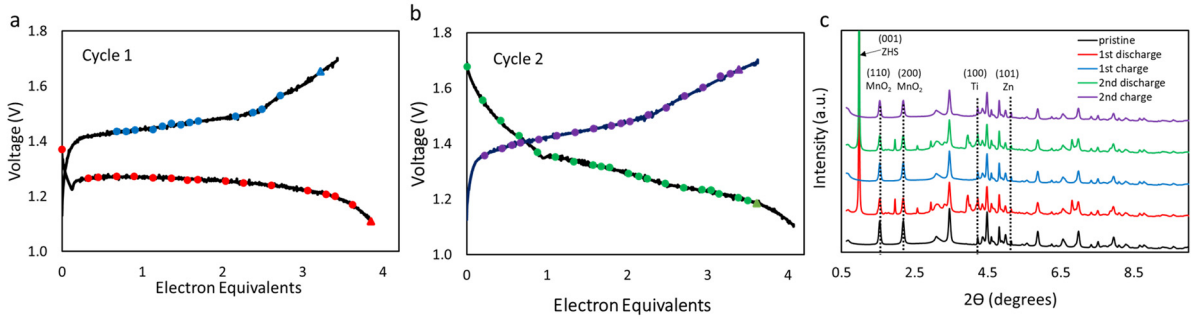

Figure S3 Synchrotron-based *Operando* X-ray diffraction (XRD) of Zn/α-MnO_2 cell during **a** Cycle 1 and **b** Cycle 2 at 50 mA/g. Colored dots represent times (state of charge) for collection of XRD patterns. **c** XRD patterns representing α-MnO_2 electrode before cycling (black) and at the end of first discharge (red), first charge (blue), second discharge (green), second charge (purple).

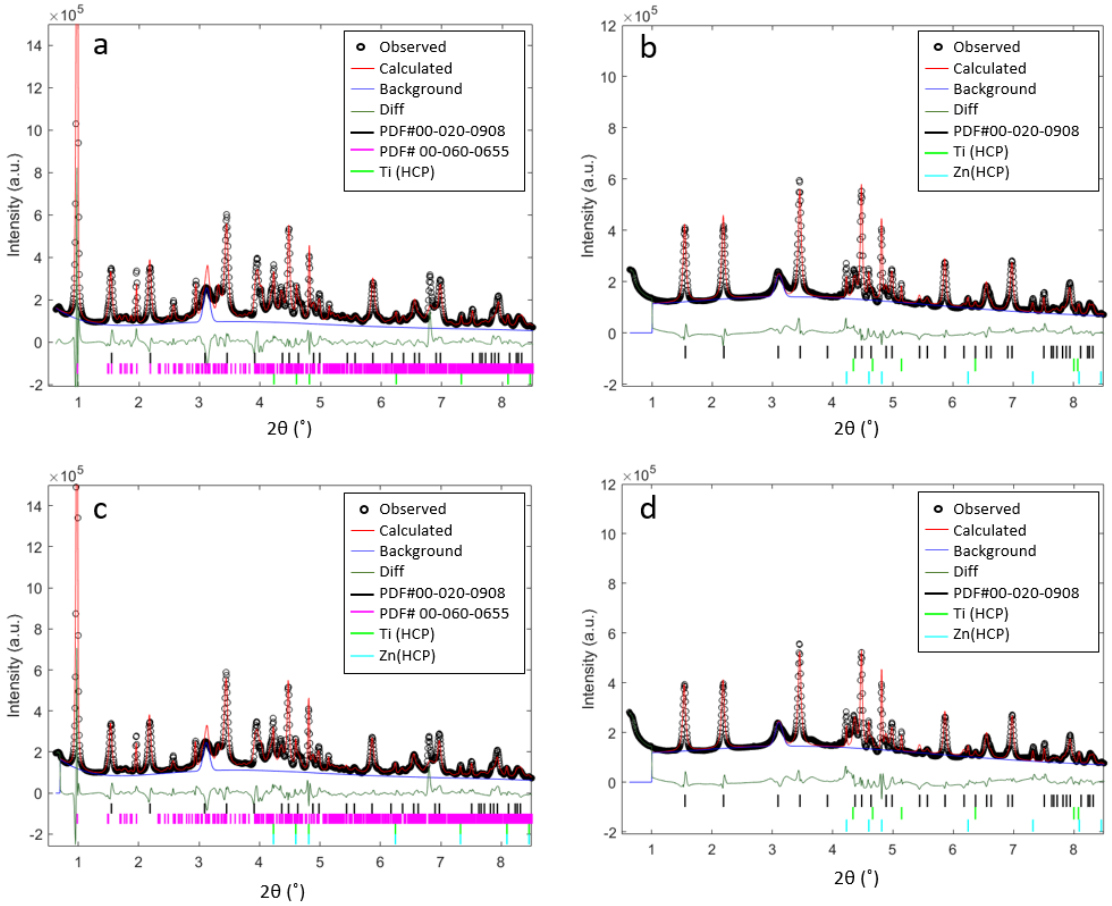

Figure S4 Rietveld refinement of **a** 1st cycle discharge, **b** 1st cycle charge, **c** 2nd cycle discharge, **d** 2nd cycle charge of the *operando* XRD cell.

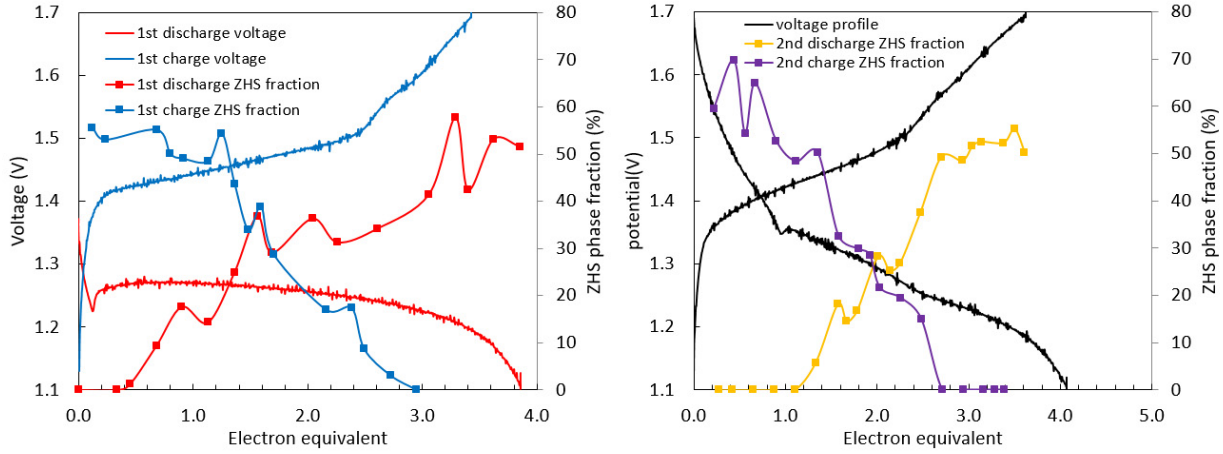

Figure S5 Voltage profile and ZHS phase fraction evolution of the *operando* XRD cell over the **a** first cycle and **b** second cycle

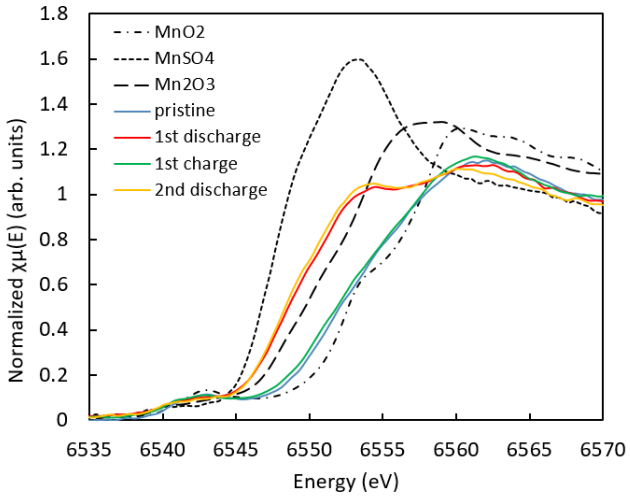

Figure S6 XANES spectra overlay of the *operando* XAS cell at different cycling stages

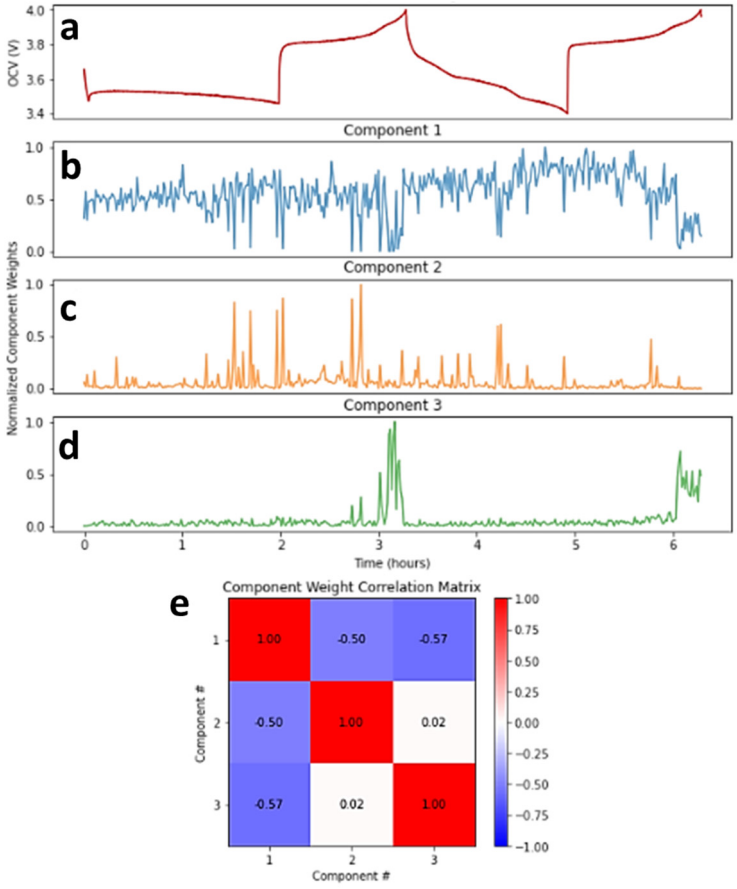

Figure S7 NMF deconvolution of operando Raman spectroscopy. **a-d** Cell open-circuit voltage vs. time during electrochemical cycling **a**, temporally aligned with normalized NMF component weights for each identified chemical species: ZHS/electrolyte **b**. cryptomelane **c**, and rancieite **d**. **e** Calculated spatio-temporal correlations between the weights of the identified NMF signal components.

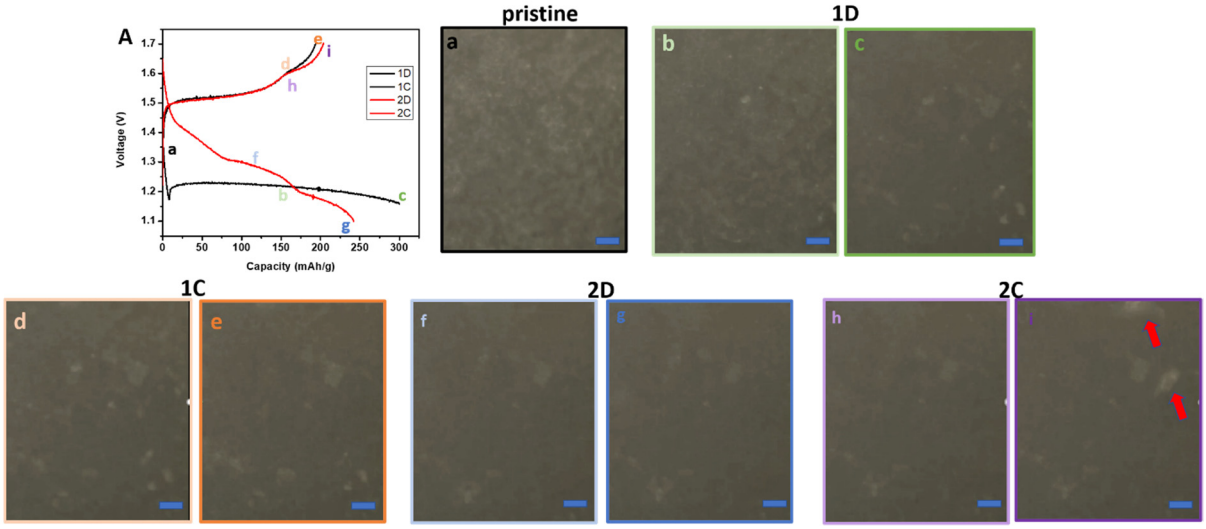

Figure S8 (A) Voltage profiles of the operando cell during the 2 cycles, as well as the optical images of the cathodes acquired at different (dis)charge states: (a) pristine, (b-c)1D, (d-e) 1C, (f-g) 2D and (h and i) 2C. The images and the corresponding time when they were captured were labeled on the voltage profiles. Scale bar= 10μm.

The optoelectrochemical testing was conducted at 150 mA/g in 2 M $ZnSO_4$ for 2 cycles, where the first discharge (1D) was Coulombically controlled to reach a capacity of 300 mAh/g. Video of the cathodes (**Video S1**, playing at 64x speed, supporting information) was recorded to capture the morphology evolution of the materials. At the pristine state (**Figure S8a**), the cryptomelane rods appeared as small white needle-like motifs. Upon the 1st discharge (1D), the morphology remained intact for the first part of the discharge (**Figure S8b**), which subsequently evolved into sheet-like morphology together with some undissolved original rods at the end of 1D (**Figure S8c**). During the 1st charge (1C), the sheet-like morphology remained during the first plateau (**Figure S8d**), and some of them dissolved by the end of 1C (**Figure S8e**). Some 2D materials seemed to be forming at the end of 1C, which can be clearly observed in **Video S1**, possibly leading to a different voltage profile in the 2nd discharge (2D). Some sheet-like materials seemed to form at earlier stage (**Figure S8f**), and the amount further increased to the end of 2D (**Figure S8g**). Similar to 1C, the sheets seemed to remain through the first plateau of the 2C (**Figure S8h**). Interesting, more 2D materials with large lateral size were formed at the end of 2C (**Figure S8i**), as highlighted by the red arrows. To provide some structural information regarding the as-formed 2D materials, ex situ Raman in combination with the optical images of the materials formed on the graphene current collector were displayed in **Figure S9**. The ex situ Raman spectra of the deposited 2D materials on the graphene current collectors confirmed the formation of the layered MnO_x phases.

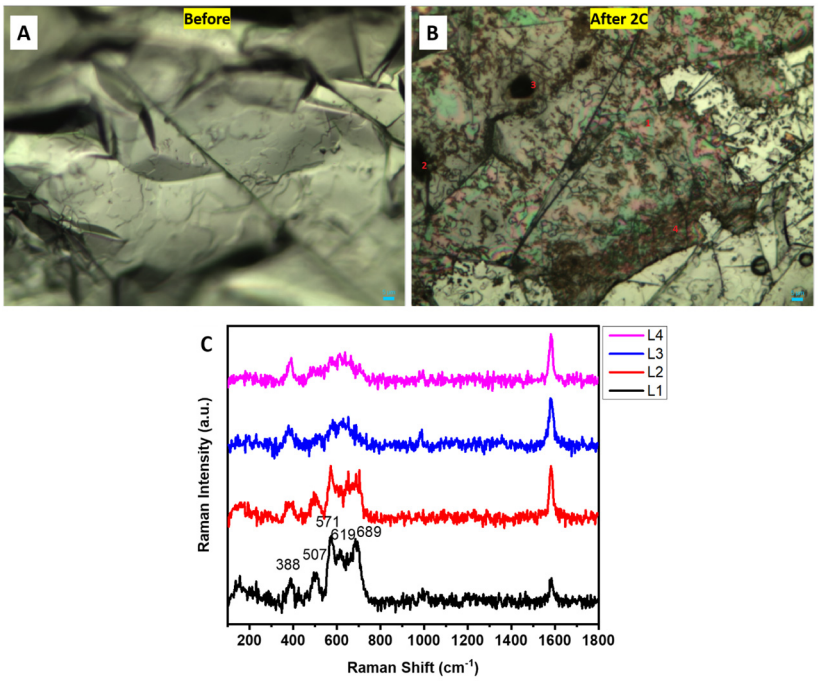

Figure S9 (A) Pristine graphene paper current collector before the operando optoelectrochemical testing. (B) Graphene paper current collector after 2C with four locations highlighted for ex situ Raman measurements. (C) Raman spectra collected at the locations highlighted in Figure B.

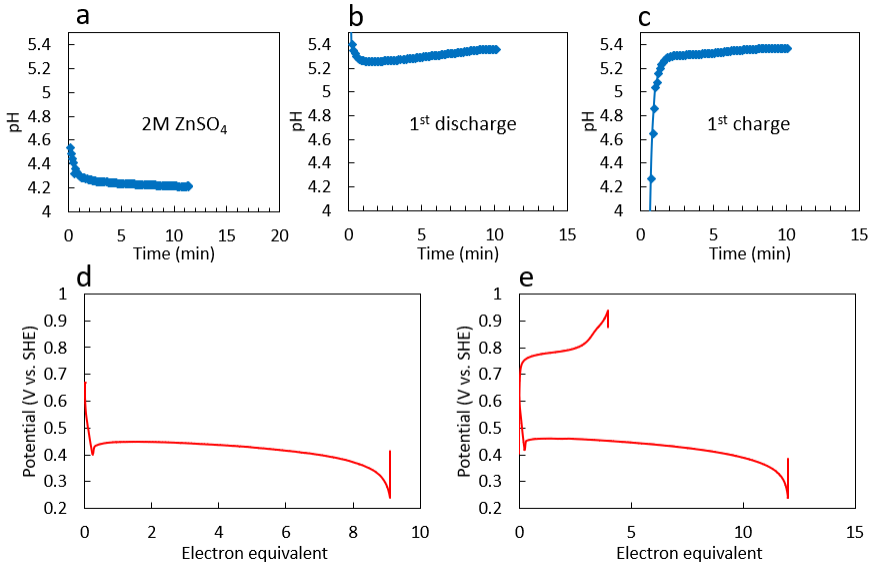

Figure S10 *in-situ* pH measurement results of **a** pristine 2 M $ZnSO_4$ electrolyte, **b** electrolyte at 1st discharge, **c** electrolyte at 1st charge, with corresponding electrochemistry **d** first cycle discharge and **e** first cycle discharge & charge.

Table S1 Rietveld Refinement results for the synthesized α-MnO_2 powder.

Parameter	α-MnO_2
Space group	I 4/*m*
a(Å)	9.817(10)
b(Å)	9.817(10)
c(Å)	2.856(15)
α=	90
β=	90
γ=	90
Crystallite size (nm)	Equatorial=25 (.02) Axial=147(32)
Weight Fraction	100%
MD ratio	1.019(.01)
%Rwp	4.337

Table S2 Rietveld Refinement results for 1st cycle discharge.

Parameter	α-MnO_2	ZHS	Ti(HCP)	Zn(HCP)
Space group	I 4/*m*	P-1	P 63/mmc	P 63/mmc
a(Å)	9.847(3)	8.36(1)	2.9368(8)	2.664(2)
b(Å)		8.37(1)		
c(Å)	2.864(5)	11.05(1)	4.675(1)	4.955(6)
α=		94.53(9)		
β=		82.95(6)		
γ=		120.02(3)		
Crystallite size (nm)	Equatorial=19 (.8) Axial=171(168)	Equatorial= 32(3.8) Axial= 307(71.7)	1000	1000
Weight Fraction	42.5%	53.1%	4.0%	0.4%
MD ratio	1.159(.01)	1.049(.0065)	1.0	1.0
%Rwp	10.521			

Table S3 Rietveld Refinement results for 2nd cycle discharge.

Parameter	α-MnO_2	ZHS	Ti(HCP)	Zn(HCP)
Space group	I 4/*m*	P-1	P 63/mmc	P 63/mmc
a(Å)	9.850(3)	8.36(2)	2.9364(7)	2.663(2)
b(Å)		8.36(2)		
c(Å)	2.8644(5)	11.06(1)	4.676(1)	4.964(6)
α=		94.6(1)		
β=		82.91(8)		
γ=		120.00(4)		
Crystallite size (nm)	Equatorial=20(.5) Axial=259(320)	Equatorial=17(.9) Axial=94(3)	1000	1000
Weight Fraction	44.8%(.6)	50.3%(1)	4.4%(.1)	0.4%(.06)
MD ratio	1.161	1.049	1.0	1.0
%Rwp	9.851			

Table S4 Rietveld Refinement results for 1st cycle charge.

Parameter	α-MnO_2	Ti(HCP)	Zn(HCP)
Space group	I 4/*m*	P 63/mmc	P 63/mmc
a(Å)	9.847(2)	2.938(6)	2.666(1)
c(Å)	2.865(3)	4.6774(9)	4.956(3)
Crystallite size (nm)	Equatorial=21(.5) Axial=157(75)	1000	1000
Weight Fraction	88.6%(7.4)	10.5%(2.5)	0.9%(.1)
MD ratio	1.117(.0056)	1.0	1.0
%Rwp	6.854		

Table S5 Rietveld Refinement results for 2nd cycle charge.

Parameter	α-MnO_2	Ti(HCP)	Zn(HCP)
Space group	I 4/*m*	P 63/mmc	P 63/mmc
a(Å)	9.847(2)	2.9383(6)	2.664(1)
c(Å)	2.8657(3)	4.6796(9)	4.963(3)
Crystallite size (nm)	Equatorial=21(.4) Axial=758(1800)	1000	1000
Weight Fraction	90.3%(.9)	8.6%(.1)	1.1%(.09)
MD ratio	1.177(.0064)	1.0	1.0
%Rwp	7.764		